communications earth & environment

Article

https://doi.org/10.1038/s43247-025-02029-2

Ecosystem changes after Early Cretaceous seawater intrusion into the proto-South Atlantic Ocean

Jian Ma[1,2] ✉, Leonardo F. Cury[3], Anelize M. B. Rumbelsperger[3], Heidi L. Albrecht[4], Erwin W. Adams[5], Joachim E. Amthor[6], Xingqian Cui[2], Antoine Crémière[7,8], Kei Sato[9], Kristin D. Bergmann[1] & Roger E. Summons[1] ✉

The early evolution of the South Atlantic Ocean following the Cretaceous break-up of Gondwana is extensively recorded in rift basins along the conjugate margins of Africa and Brazil. For the Brazil side, divergent views of the source and pathway of the initial seawater incursion persist due to a paucity of recognized transitional sequences that document marine transgressive deposits over the continental interior. To address this, we conducted a high-resolution sedimentological and geochemical study through a core in the Campos Basin that encompasses the key lithologic switch from lacustrine carbonate to marine evaporite settings. Steroid lipid biomarkers, derived from pelagophyte marine algae, make a striking appearance in concert with a pronounced negative shift of $^{87}Sr/^{86}Sr$ ratios and coincident with the appearance of anhydrite. Importantly, the sulfur-sequestered biomarkers reveal a dynamic system where redox-stratified and anoxic conditions were amplified along with a deepening chemocline through the marine transition.

The Early Cretaceous breakup of the western Gondwana Supercontinent marks the birth of the South Atlantic Ocean (SAO) and instigated a range of other impacts on the Earth system[1–5]. Specifically, the Aptian–Albian stage is a critical interval in terms of the development of a new oceanic gateway and the initiation of the central SAO between the rifting South America and Africa plates[6–9]. As a consequence, seawater ingress along with marine organisms transformed the pre-existing saline lacustrine ecosystems[10]. The widespread Aptian–Albian sea/seaways in the plate interiors led to the development of restricted and hypersaline environments[11] and ubiquitous thick deposits of salt with organic-rich layers along the Brazilian-African conjugate margins[11,12]. Concomitantly, the Aptian–Albian transgression was sufficiently extensive to induce the propagation of marine biota[13–15]. In turn, sedimentary and fossil records in the conjugate margins of Brazil and West Africa provide fundamental constraints useful for paleogeographic reconstruction. Despite numerous reports of marine incursions, however, there are divergent views on the source and pathways taken by the first marine transgression into these intracratonic basins, hindering our understanding of paleogeographic and ecosystem reconstruction (Supplementary Fig. 1). On the Brazil side, it is postulated that a long-distance Aptian–Albian transgression, originating from the equatorial Atlantic Tethyan Ocean, spread southwards[8], while tectonic evolution analyses support northward Aptian–Albian marine ingressions from the austral SAO[16–19]. Pathways of marine ingressions are further complicated by conflicting results based on paleocurrent data and fossil marine biota comparisons between NE and SE Brazilian basins[7,20]. The conundrum persists, as the paucity of transitional sedimentary sequences that represent marine transgressive deposits over the continental interior hinder the interpretation of ecosystem impacts.

Discriminating between non-marine and marine-influenced settings, especially in the absence of body fossils, is heavily reliant on sedimentology and geochemistry. Even so, much of the available toolkit is unable to unequivocally discriminate between marine and saline lacustrine deposition. Conversely, fossil lipids—biomarkers—represent geologically stable molecules derived from the diagenetic modification of microbially-derived precursors thereby fingerprinting parent organisms and, by extension, the depositional environment they once inhabited[21–23]. Of particular

[1]Department of Earth, Atmospheric and Planetary Sciences, Massachusetts Institute of Technology, Cambridge, MA, USA. [2]School of Oceanography, Shanghai Jiao Tong University, Shanghai, China. [3]Federal University of Paraná, LAMIR Institute, Curitiba, Paraná, Brazil. [4]Shell Exploration and Production Company, Houston, TX, USA. [5]Shell Global Solutions International BV, The Hague, The Netherlands. [6]Division of Earth Sciences and Geography, Rhine-Westphalia Technical University of Aachen, Aachen, Germany. [7]Division of Geological and Planetary Sciences, California Institute of Technology, Pasadena, CA, USA. [8]Geo-Ocean, Univ Brest, CNRS, Ifremer, UMR6538, F-29280 Plouzané, France. [9]São Paulo University, São Paulo, São Paulo, Brazil. ✉e-mail: majian_geo@sjtu.edu.cn; rsummons@mit.edu

significance here is 24-*n*-propylcholestane (24-npc), a steroidal lipid derived from the diagenetic transformation of 24-*n*-propylcholesterol—the major sterol constituent of modern marine pelagophyte algae[24]. Given that contemporary pelagophyte algae are exclusively marine organisms, and the ubiquity of 24-npc in Mesozoic-Cenozoic marine-derived organic matter [25,26], 24-npc is widely applied as a diagnostic indicator of marine-influenced sedimentation[27–29]. Hitherto, most biomarker-based paleoenvironmental interpretations have focused on 'free' lipids from organic extracts of rocks. On the other hand, chemolysis studies have demonstrated that organic molecules with multiple unsaturations (double bonds) and/or particular functional groups are prone to rapidly react with reduced inorganic sulfur species (e.g., H_2S) under anoxic and sulfidic conditions to become incorporated via S-S and S-C crosslinking into the polar or macromolecular fractions of sedimentary organic matter[30,31]. Therefore, organic sulfurization can lead to selective sequestration of specific biomarker precursors affording investigation of diverse complex species that are not readily amenable to conventional lipid analysis[32–34] and which can resolve biases in paleoenvironmental reconstruction[35,36]. Given widespread anoxic environments in Aptian–Albian strata of Brazilian marginal basins[7,11], both free and sulfurized lipids of organic extracts need to be evaluated before a complete biomarker picture can be visualized.

In an independent yet complementary approach, the radiogenic Sr isotopic composition ($^{87}Sr/^{86}Sr$) of sediments is sensitive to the weathering inputs into a basin. In a lacustrine environment, the $^{87}Sr/^{86}Sr$ isotopic composition is set by the radiogenic $^{87}Sr/^{86}Sr$ isotopic of the specific combination of bedrock within upstream catchments. In the case of the Brazilian lacustrine systems, it has been postulated that extremely radiogenic Precambrian cratonic bedrock on both the South American and African margins determined the $^{87}Sr/^{86}Sr$ isotopic composition of the lacustrine rift system[37,38]. In contrast the $^{87}Sr/^{86}Sr$ isotopic composition of marine waters is well mixed and yields a coherent marine $^{87}Sr/^{86}Sr$ isotope curve through time[39]. Reconstructing the $^{87}Sr/^{86}Sr$ isotopic composition of South Atlantic sediments can, therefore, yield an independent record of marine transgression into the lacustrine system.

Herein, we report free and sulfurized lipid biomarkers and Sr isotope analyses, along with carbon, oxygen, and clumped isotopes and sedimentological descriptions of a core retrieved from the SE Brazilian Campos Basin that reveal the initial Aptian marine ingress therein and associated ecosystem reorganization. The succession cored by the Fragata borehole, located close to the center of the southern Campos Basin (Fig. 1), encompasses lacustrine carbonates of the upper Macabu Fm. and interbedded anhydrite, halite and carbonate rocks of the Retiro Fm., thus providing a sedimentological record and opportunity to explore preserved organic matter associated with the event. Our findings address the knowledge gap about the impact of the marine transgression in the western conjugate margin by documenting its environmental consequences and ecosystem responses.

Results and discussion

Seawater ingress into the Campos Basin

The Macabu Fm. in the Campos Basin is dominated by carbonate successions, which developed in an alkaline lacustrine setting under an arid climate[40–42]. The overlying Albian aged Macaé Group in the Campos Basin clearly records sedimentation in a marine environment, as evidenced by foraminiferal biozonation and carbonate microfacies[43]. Contrastingly, the Retiro Fm. is typified by evaporites, which represents the transitional phase between successions in the Macabu Formation and the Albian-aged Macaé Group, and may record the initial marine incursions in the Campos Basin.

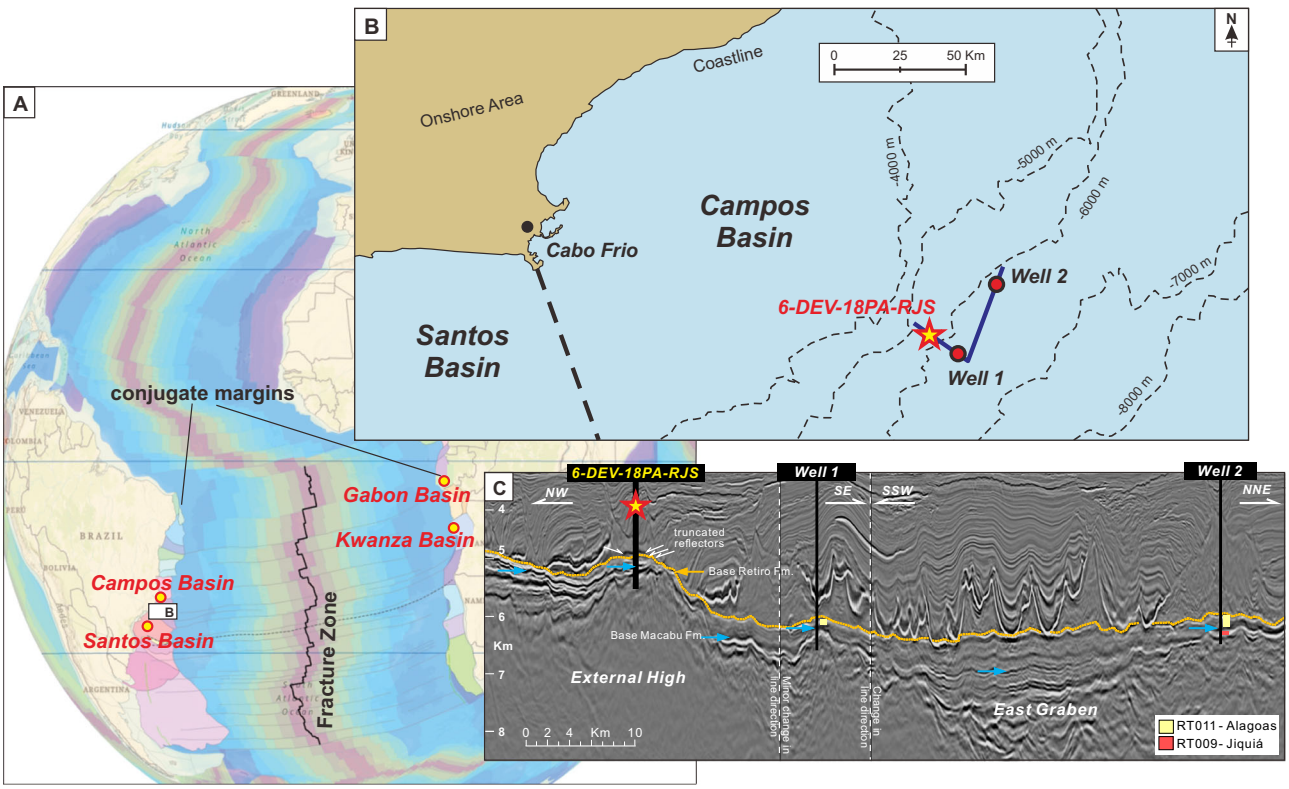

Fig. 1 | Geological maps with locations of the Campos Basin and Fragata drill core. The location of the Fragata drill core within the geological map of the Campos Basin (**B**) in the Brazilian conjugate margin (**A**). The geological map illustrates the present-day coastline as well as depth contours in meters for the top of the Macabu Formation (**B**). Northwest to southeast with change in dip direction to north-northeast seismic section (blue lines in **B**) in depth illustrating the geologic context of the Fragata core (6-DEV-018-RJS) in the Campos Basin (**C**). Blue arrows indicate the base of the Macabu Formation; The orange arrow and dotted line show the base of the Retiro Fm. The Fragata core is located at the edge of the external high with seismic reflector terminations (white arrows) indicating erosion along an escarpment setting. Outboard parallel, continuous reflectors are observed indicating a ponded and deeper lake system. Two wells (Well 1 and 2) located in the East Graben in the outboard comprise pre-salt ostracod biostratigraphic data and calibrate the stratigraphy to the Jiquiá and Alagoas zones or Coqueiros and Macabu Formations, respectively. Sources of the basemap (**A**): Esri, HERE, Garmin, FAO, NOAA, USGS.

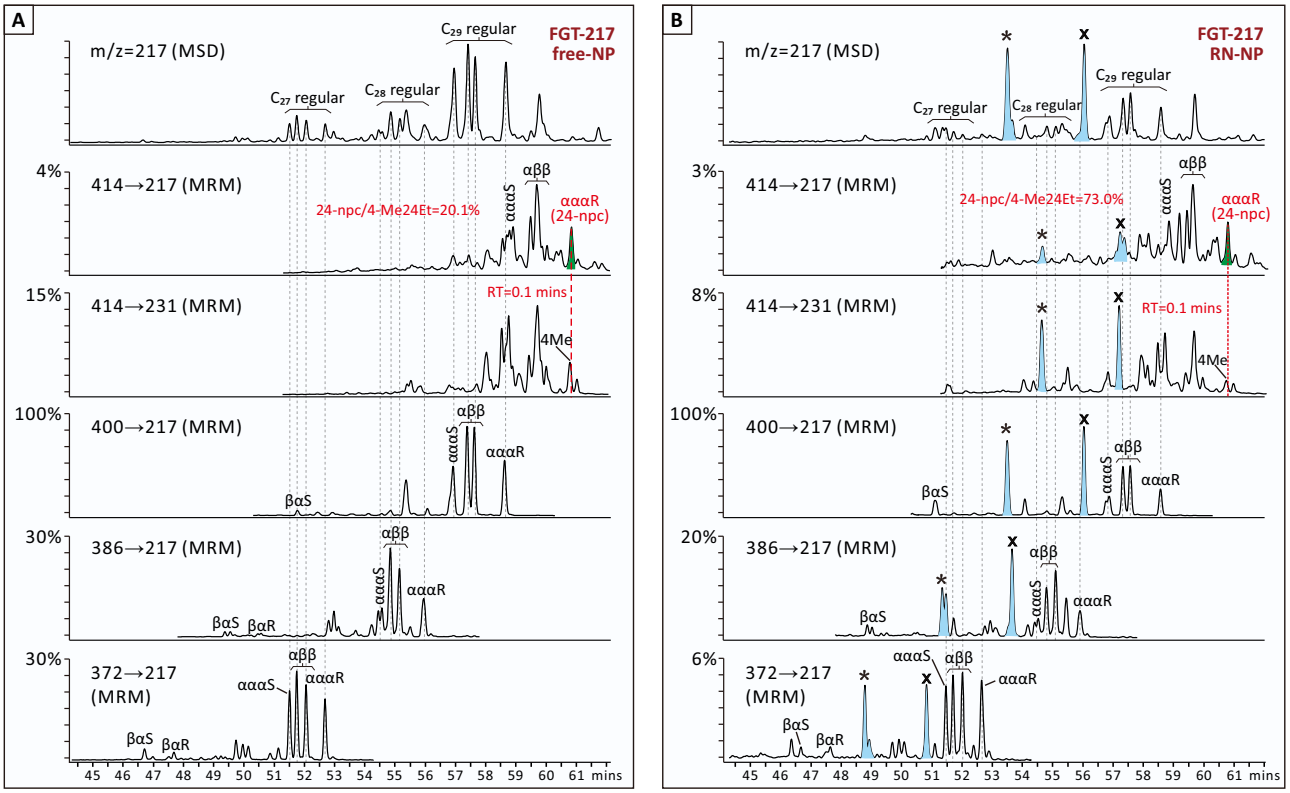

Fig. 2 | Sterane composition in free and desulfurized lipids for sample FGT 217 (5020.48 m). The marine algal signal can be detected in both free (free-NP, free non-polar fractions, **A**) and RN (RN-NP, non-polar fractions obtained by Raney Ni treatment of polar fractions, **B**) fractions of rock extracts in samples above 5025 m (e.g., FGT 217). Here, the chromatograms at the top of the (**A**, **B**) stacks show *m/z* 217 from full scan GC-MSD data. Chromatograms for individual sterane carbon numbers are from GC-QQQ data; scales in each chromatogram are normalized to the highest peaks (shown as 100%). Peaks of 24-npc (24-*n*-propylcholestane, green peaks) are highlighted with red dashed line, with the reproducible offset of retention time at ~0.1 min compared to the peaks of 4-Me24Et (4α-methyl-24-ethylcholestane). 24-npc ratios (24-npc/4-Me24Et) are 20.1% and 73.0% in free-NP and RN-NP fractions, respectively. Additionally, unconventional configurations of C_{27}-C_{30} steranes, which are denoted as 5α,14α,17β(H) 20 R (ααβ, blue peaks marked with * in the right panel) and 5α,14β,17α(H) 20 R (αβα, blue peaks marked with **x** in the right panel) (Fig. S8), were identified in this study. They are mostly detected in RN-NP fractions of marine influenced samples in the Fragata core and are predominant among all steranes. The identification of ααβ and αβα steranes are based on mass spectra (Fig. S8)[91] and retention times[92]. Abbreviation: free-NP free non-polar fractions, RN-NP non-polar fractions by Raney Ni treatment on polar fractions.

Both carbonate clumped isotope (Δ47) values and the stereochemical configurations of biomarkers reveal a moderate thermal history for the study area (SI). A wide array of lipid biomarkers, including *n*-alkanes, acyclic isoprenoids, terpanes, steranes, hopanes and carotenoids, were characterized in both free and desulfurized fractions (Supplementary Fig. 6) isolated from the Fragata core samples (Fig. 1). Of particular significance among the sterane biomarkers is the detection of 24-*n*-propylcholestane (24-npc) in both free non-polar (free-NP) and a complementary set of non-polar fractions generated by Raney Ni desulfurization (RN-NP) (Fig. 2). As a geological derivative of 24-*n*-propylidenecholesterol[24,25], 24-npc is the major sterane diagnostic for marine chrysophyte/pelagophyte algae[44,45]. Accordingly, 24-npc is ubiquitously detected in marine environments and has been widely adopted as a diagnostic marker of marine or marine-influenced strata in the geological record[26–29,46]. There 24-*n*-propylidenecholesterol, the likely precursor of 24-npc through diagenesis, has been found in a specific member of foraminifera (e.g., *Allogromia laticollaris*)[47], however, the low abundance of 24-*n*-propylidenecholesterol synthesized by foraminifera cannot account for the concentration of 24-npc detected in the Fragata samples. The detection of 24-npc may be confounded when in low relative abundance due to an interference signal from 4α-methyl-24-ethylcholestane (4α-methylstigmastane, 4-Me24Et)[21] that partially co-elutes on most GC liquid phases. Strict criteria are followed for the rigorous identification of 24-npc in the Fragata samples and include the relative signal intensities and the small but reproducible retention time difference between isomers of 24-npc and 4α-methyl-24-ethylcholestane[27]. Ratios of the ααα-(20 R) isomers 24-npc and 4-Me24Et (denoted as 24-npc ratio) are elevated in samples shallower than 5024.3 m in the Fragata core (26.7% ± 8.8%, 1σ, Supplementary Table 2). This allows a positive identification of 24-npc, since the 24-npc/4-Me24Et ratios in seawater-influenced settings are expected to exceed 10%[21,28]. Additionally, a reproducible offset[27] of ~0.1 mins in the chromatographic peaks in the 414 → 217 and 414 → 231 Da transitions on GC-QQQ-MS (Fig. 2) further verified the marine signature of 24-npc at the top of the Fragata core. Significantly, 24-npc peaks are also recognized in the desulfurized RN-NP fractions (Fig. 2) with elevated signal intensities. Above 5024.3 m the 24-npc ratios rise to 73.0% (51.8% on average, Supplementary Table 2). Accordingly, the occurrence of 24-npc in both free and sulfurized fractions, restricted to the entire interval above 5024.3 m in Fragata core, and upwards from the first appearance of anhydrite at the base of the Retiro Fm. indicates that marine waters had intruded into Campos Basin during the late Aptian (<116 Ma).

Notable variations of $^{87}Sr/^{86}Sr$ were captured in the interval above 5024.3 m in the Fragata core (Fig. 3). The findings delineate distinct groups characterized by ratios falling within the ranges of 0.712–0.714 and 0.709–0.710. The initial interval, previously identified in several studies[40,48,49], is attributed to distinctly continental sources, serving as a significant geochemical indicator supporting the interpretation of the carbonate succession as having a lacustrine origin in the Campos and Santos basins. Despite the limited understanding of the paleo-tectonic context, the notable variability in the strontium isotope signal indicates a depositional system influenced by a range of sources, including continental cratonic rocks and contemporaneous basaltic volcanism as potential contributors[37,50]. The second interval, however, exhibits notably reduced radiogenic Sr values, predominantly around 0.709, indicating a distinct decrease in radiogenic sources entering the basin. Influx of marine waters

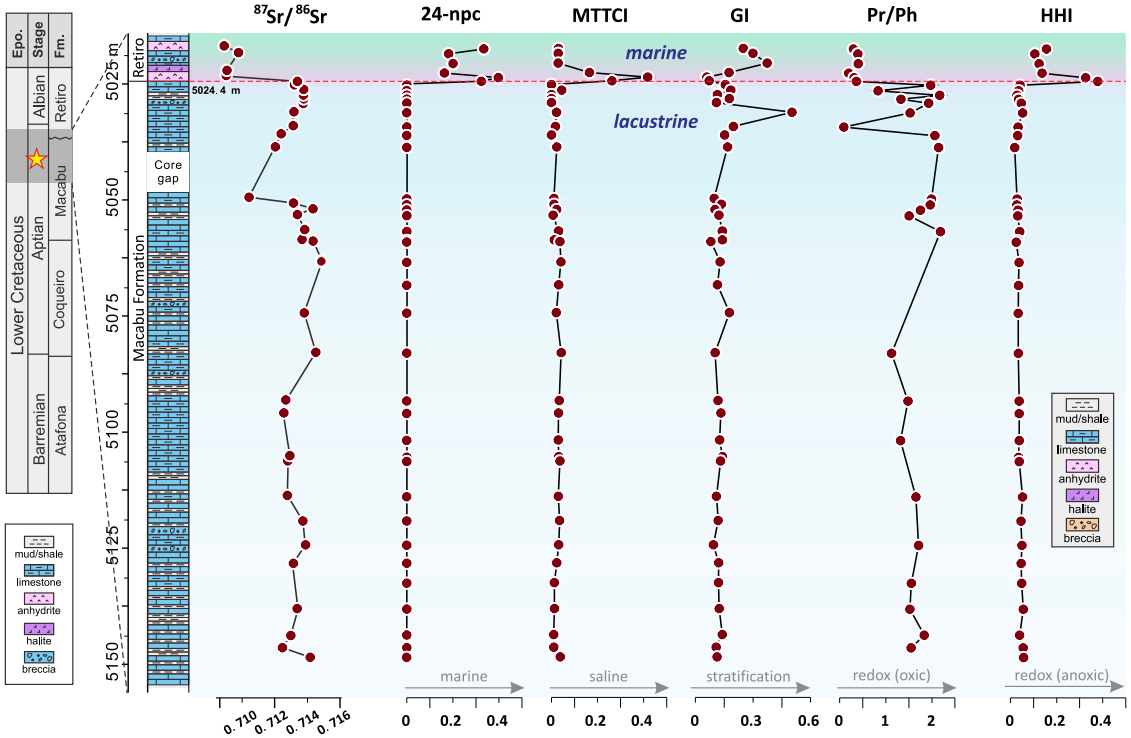

Fig. 3 | Lithostratigraphic framework of the Fragata core. Sr isotope and biomarker profiles of the Fragata core spanning the Upper Macabu Formation through the Lower Retiro Formation from 5017.3 m to 5048.7 m. 24-npc = 24-*n*-propylcholesterane (24-npc)/4-methylsterane, MTTCI = Methyl MTTC (Methyltrimethyltridecylchromans)/trimethyl MTTC, GI = gammacerane/C_{30} αβ hopane, Pr/Ph = pristane/phytane, HHI = C_{35} homohopanes/C_{30} αβ hopane.

would be reasonable, given that the anticipated average $^{87}Sr/^{86}Sr$ ratio for seawater during the Aptian period is approximately 0.707[51]. Additionally, the strontium isotopes of early marine deposits in the Campos Basin show similar ranges (e.g., 0.7074–0.7077)[43], which is clearly distinct from the isotopic composition of the lower interval in our study (e.g., 0.712–0.714). A mix between internally drained solutes and marine influx would produce a hybrid brine with a new $^{87}Sr/^{86}Sr$ ratio under hydrological equilibrium. Considering fluctuations in water levels within a shallow environment, with a water/Sr mass balance sensitive to source variations, it may be possible to explain the variation in radiogenic strontium within the Macabu Formation due to changes in sources that are influenced by tectonic activity. The excursions of $^{87}Sr/^{86}Sr$ ratio are indicative of sources related to mafic volcanic rocks and/or marine incursions. While other strontium excursions are observed in the lower intervals of the pre-salt carbonates[48,52], a significant shift at the top of the succession, concordant with the contact with the Retiro Formation, suggests this point as the onset of predominant marine influx.

Paleontological evidence has implied that seawater infiltrated from the NE Brazilian marginal basins, including the Sao Luís, Parnaíba and Araripe basins during the transition of Aptian–Albian; Furthermore, a Tethyan ingression is suggested by the presence of several fossil taxa[8,13–15]. Likewise, the Tethyan affinities of plankton in the Kwanza Basin indicate the southward advection of surface water in the northern South Atlantic[53]. However, there is a lack of unequivocal marine evidence in the SE Brazilian marginal basins (e.g., Campos and Santos Basins). Accordingly, a series of southward marine transgressions from the equatorial Tethys Ocean was hypothesized[7,8] divergent from the tectonic evidence of a marine pathway extending from south to north on the basis of sea-floor spreading patterns and geodynamic reconstructions[16–19], recently acquired geochronological data[37,50] and from evidence gathered from the conjugate margins of West Africa[9].

A switch to a marine-influenced ecosystem

Numerous examples have illustrated how seawater entry into lacustrine ecosystems alters their hydrography, water chemistry and biology. Ingressions can result from subtle changes in relative sea level on glacial-interglacial timescales (e.g[54].) or from tectonism on geological timescales[27–29,54]. The salinity and depth of a water body, together with basin shape, will influence the tendency towards density stratification. Relative abundances of methyltrimethyltridecylchromans (MTTCs) isomers (e.g., methylated MTTCs) have been proposed to be a reliable indicator for paleosalinity in aquatic surface-layers[55,56], especially recording the periodic incursions of marine waters and subsequent evaporation[57]. Here, the Fragata core records enhanced MTTCs ratios (0.02 vs. 0.16 on average, with the highest value to 0.42, Supplementary Table 2, Fig. 3), pointing to a rapid elevation in salinity above 5025.12 m. Subsequently, the elevated abundance of gammacerane (denoted by the gammacerane index, GI) is additionally indicative of enhanced water column stratification, given that its precursor, tetrahymanol, is a signal for bacterivorous ciliates living at redox transitions[58,59]. Stratification reduces mixing and thus promotes oxygen-depletion in deeper waters, as evidenced by concomitant reduction in the pristane/phytane (Pr/Ph) ratio and enhancement of C_{35} Homohopane Index (C_{35} HHI) at the top of the section (Fig. 3). Pr/Ph is regarded as a redox-sensitive proxy due to the preferential formation of phytane over pristane derived from the phytol side-chains of chlorophylls under anoxic conditions[60]. Although additional factors including salinity, organic matter sources, and diagenetic process may affect Pr/Ph[61,62] values below 1 are considered diagnostic for pervasive anoxia. Similarly, the C_{35} HHI is a robust proxy for tracing anoxic conditions[21], considering that the C5 side-chains of its precursor compounds, C_{35} bacteriohopanepolyols, are best preserved under the anoxic and H_2S-rich conditions that follow from enhancement of sulfate levels from seawater incursions[63,64]. Together, the evolution of multiple biomarker proxies documents a hydrographically dynamic system, capturing the establishment of enhanced anoxic/euxinic, saline, and stratified conditions in the Retiro Formation. Additionally, we observed a delay of the enhancement of GI intensity than HHI (Fig. 3). We postulate that the stratification increased progressively before the new marine-dominated microbial community became established. The sulfur-sequestration of lipids representing the biotic transformation, on the other

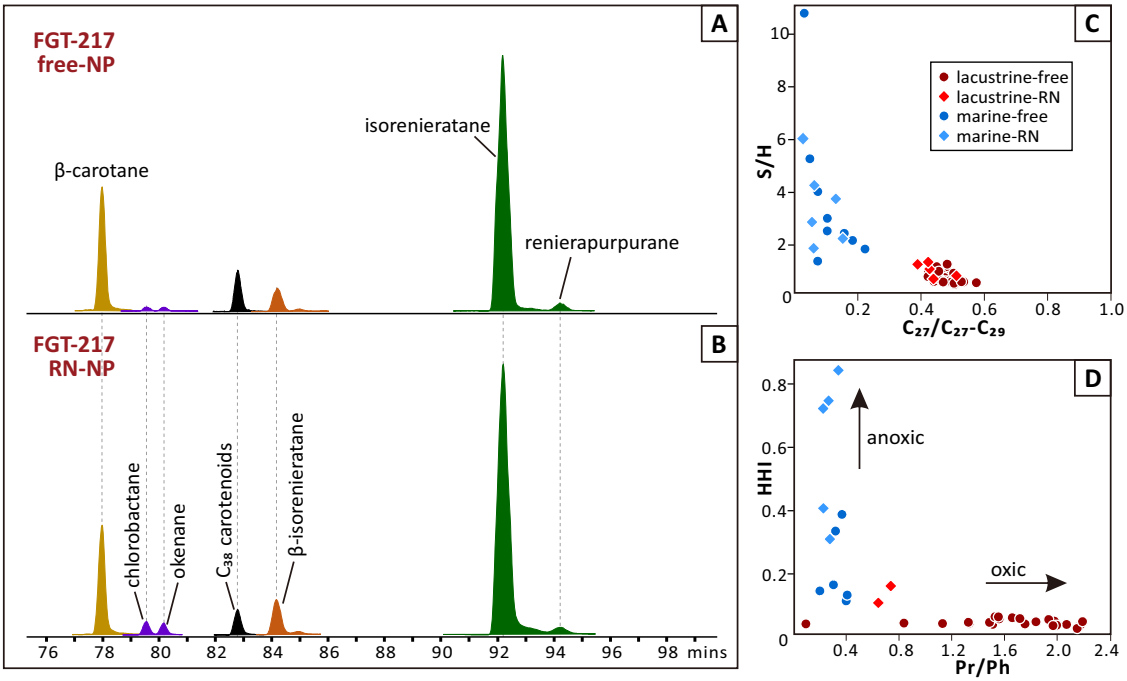

Fig. 4 | Biomarker comparisons of free and desulfurized lipid fractions. A, **B** As shown in the sample FGT-217 (5020.48 m), there are distinctive abundances of PSB-specific and GSB-specific carotenoids (i.e., okenane and chlorobactane respectively) after the desulfurization treatment; **C**, **D** All marine-influenced samples are characterized by anoxic (high HHI and low Pr/Ph) and eukaryote dominance indicated by a high S/H and with C_{29} sterane predominance.

hand, was geologically instantaneous, considering that organic sulfurization is a facile and rapid process[65–67].

Given the enhancement of anoxia induced by the marine incursion, reductive sulfurization of organic matter under euxinic conditions[33] becomes an issue that may complicate or inhibit the identification of some biological precursor lipids[68]. In fact, here, the patterns of *n*-alkanes, and of sterane and hopane stereoisomers released by the RN treatment (Supplementary Fig. 6 and 7), illustrate how specific biomarkers have been sequestered into the S-bound macromolecular component of sedimentary organic matter. High abundances of phytane and C_{35} homohopanes released during desulfurization (Fig. 4D) further confirm their preferential preservation under anoxic and sulfidic conditions[60,64]. Despite striking differences in the patterns of the free-NP and RN-NP fractions, however, the key biomarker proxies all move in a consistent direction concomitant with the marine incursion. Both free and sulfurized lipids also reveal a dynamic system: Here, the ingress of seawater strengthened stratification within this sector of the Campos Basin, fostering the development of water column anoxia, as evidenced by elevated values of GI, C_{35} HHI and MTTC (Fig. 5). Accordingly, hydrographic changes induced by seawater ingress have prompted ecosystem re-structuring as recorded in its biochemostratigraphy. A striking and progressive elevation in sterane/hopane ratios (S/H) (up to 10.6, Supplementary Table 2), a proxy based on the diagenetic products of sterols and hopanoids diagnostic for eukaryotes and bacteria respectively[21,69], suggests this environmental shift appears to have favored photosynthetic algae, allowing their proliferation at the expense of cyanobacteria. Consistent with transgressive records in other basins[23,27], the elevated S/H document the ingress of seawater providing algae with an advantage over the bacterial community whether by addition of nutrients or other factors associated with the water chemistry (e.g., trace elements). Among all steroid derivatives, stigmastane (C_{29} sterane) becomes dominant over cholestane, its C_{27} counterpart, after the marine incursion (Fig. 4C; Fig. 5). Given their mostly biological source from Chlorophyceae and Rhodophyceae, respectively[70,71], the enhanced stigmastane represents the likely prevalence of green algae over other taxa in the immediate aftermath of the transition.

A progressive deepening of the chemocline with marine ingress

Despite the detection of the array of carotenoid pigments in the free biomarker fractions (Supplementary Table 2), diverse inventories of aliphatic and aromatic carotenoids are released upon desulfurization of the polar fractions (Fig. 4A, B). In the free-NP fractions, the predominant compounds in all samples are β-carotane and isorenieratane, together with minor β-isorenieratane and C_{38} carotenoids. However, in the RN-NP fractions, relatively high abundances of isorenieratane, chlorobactane and okenane that have been sequestered into macromolecules by sulfurization supports the notion that they represent indigenous signals for phototrophic sulfur bacteria. As strict anaerobes, these phototrophic sulfur bacteria, comprising green sulfur bacteria (i.e., GSB, *Chlorobiaceae*) and purple sulfur bacteria (i.e. PSB, *Chromatiaceae*), utilize sulfide and other reduced sulfur species as electron donors for photosynthesis[72]. Because of their dual requirements for illumination and sulfide, the GSB and PSB are considered index species for photic zone euxinia (PZE) where the light penetrates a sulfide-containing water column[73]. Thus, their biomarker lipids have been applied as PZE biosignatures in both modern environments and in paleoenvironmental reconstruction[68,69,74–77]. Being the most widely recorded aromatic carotenoid in marine sediments[75,78], isorenieratane is the diagenetic product of isorenieratene that is derived from low-light-adapted brown strains of phototrophic green sulfur bacteria (GSB). These GSB are known to be well adapted to lower light intensities and therefore deeper waters (~100 m)[73,79]. In comparison, green-colored strains that produce chlorobactene, the biological precursor of chlorobactane, require higher light intensity and accordingly are concentrated at shallower (~15–30 m) chemocline depths[80]. Okenone-synthesizing PSB can proliferate as plankton within a shallow chemocline (~20 m[81];), in benthic microbial mats, and as aggregates with sulfate reducing bacteria in the water column[82] or, perhaps reflecting their slightly higher tolerance for oxygen, as observed in the 'pink berry consortia' that are found in tidally-influenced marginal marine environments[83].

In the present study, by comparing the sedimentary lipids of the free and S-bound fractions, we observe a novel switch in the assemblages of aromatic carotenoids upon initial marine ingress into the Campos Basin. At the base of the anhydrite-bearing layer that marks the onset of the incursion, a peak in

PSB-derived okenane (up to 33.0%, Fig. 6, Supplementary Table 2) implies extremely shallow PZE or microbial mat facies. Okenane then declines coincident with a peak in the abundance of GSB-derived chlorobactane (3.8%) and elevated isorenieratane. After this, isorenieratane becomes the dominant aromatic carotenoid identifying the brown-pigmented GSB as the predominant anoxygenic phototroph and a deepening chemocline. In addition, the composition of C_{38} aromatic carotenoids decrease markedly (6.4% vs. 18.2%, $p < 0.001$, Supplementary Table 2). These C_{38} aromatic carotenoids are the diagenetic products of synechoxanthin which is a C_{40} aromatic carotenoid with dual carboxylic acid functionalities prevalent in non-marine or

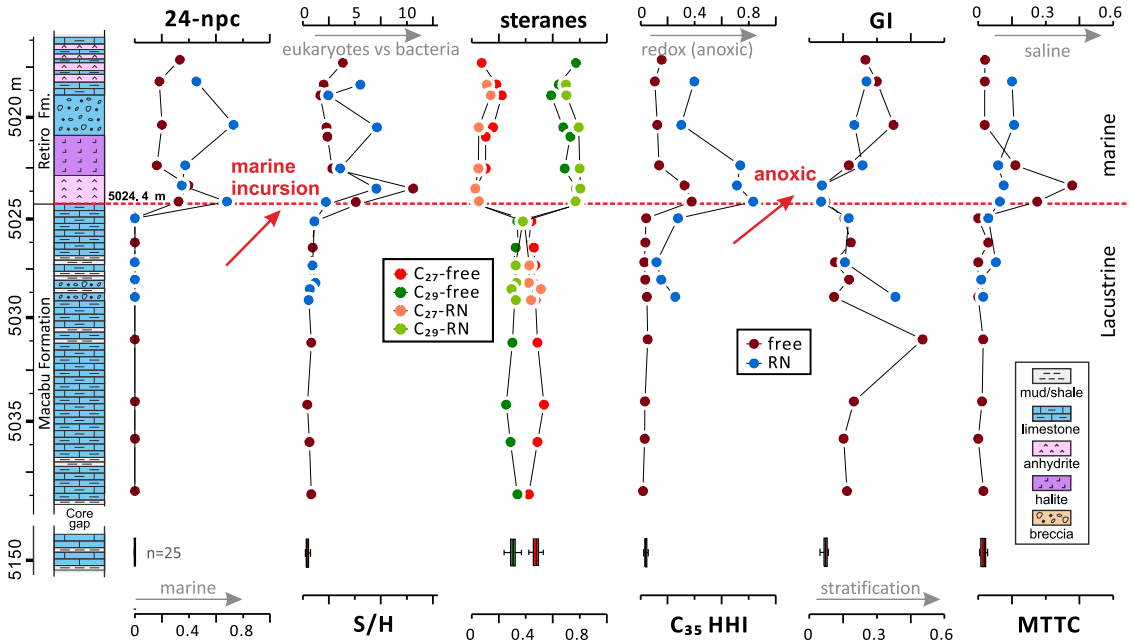

Fig. 5 | Expanded geochemical profile for the top of the Fragata core, recording the ecosystem reorganization upon ingress of seawater at <116 Ma. These changes coincide with the appearance of anhydrite in the sediment column. Both free and sulfurized biomarkers are self-consistent, especially for the detection of 24-npc, indicative of indigenous signals. 24-npc = 24-npc/4-methylsterane, S/H = C_{27}-C_{29} steranes/C_{27}-C_{35} hopanes; Steranes = C_{27} or C_{29} steranes/C_{27}-$_{29}$ steranes, C_{35} HHI = C_{35} homohopanes/C_{30} αβ hopane, GI = gammacerane/C_{30} αβ hopane; MTTC = Methyl MTTC (Methyltrimethyltridecylchromans)/trimethyl MTTC. Biomarker data from samples below 5038.58 m (n = 25) are summarized in the form of box and whisker plots.

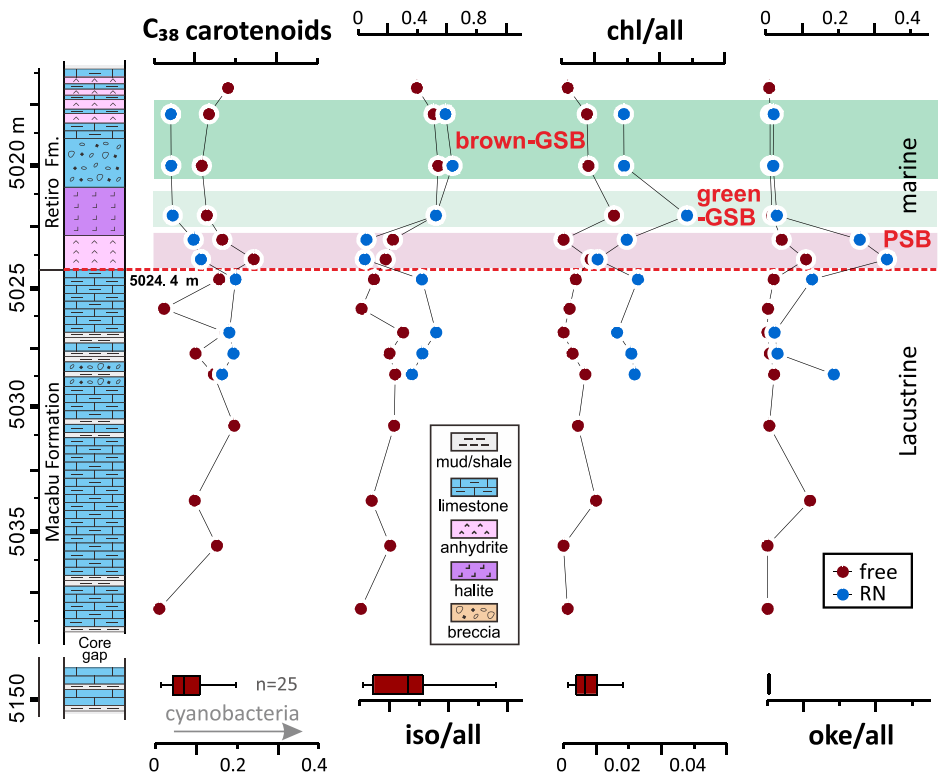

Fig. 6 | Evolving carotenoid distributions following the onset of the marine transgression captured by the upper Macabu–Lower Retiro Formations within the Fragata core. Here, horizontal shaded bars illustrate the changes in the community of phototrophic bacteria following the intrusion of sulfate-bearing marine waters. Changes in the dominant carotenoids illustrate a clear progression from okenane (oke), through chlorobactane (chl) and subsequently to isorenieratane (iso) that reveals a shift from purple sulfur bacteria (PSB) at the initial seawater ingress, through green- and then brown-pigmented green sulfur bacteria (GSB). Red and blue datapoints identify trends in free and sulfurized lipids, respectively. The box and whisker plots summarized the carotenoid data from below 5038.58 m ($n = 25$) (Fig. 2; Supplementary Table 1).

euryhaline cyanobacteria[22,74,84,85]. Thus, reductive sulfurization and decarboxylation affords the C_{38} diagenetic products together with C_{39} counterparts diagnostic for cyanobacteria that are prevalent while lacustrine conditions prevail. Their decline coincides with the increases in phototrophic sulfur bacteria that accompany the ingress of seawater. In other words, the marine incursions instigated an overturn of the photosynthetic community, including a proliferation of eukaryotic algae together with GSB concomitant with a decline in primary productivity by the synechoxanthin-producing cyanobacteria. In summary, the combination of a less radiogenic $^{87}Sr/^{86}Sr$ ratio together with 24-npc and carotenoid hydrocarbon biomarkers indicate a marine incursion associated with the deposition of the Retiro Formation, associated with a fundamental transformation in the biological community.

Materials and Methods

Petrology inspection and organic extraction

In total 40 core samples of carbonates and mudstones, with a 2–4 m resolution of depths, were selected from the Fragata core in the Campos Basin (Fig. 1A, B) covering a depth range of 5026.320 m to 5148.695 m (Fig. 1B, red dots). The age model of the Fragata core is based on the age constraint provided by a LA-ICP-MS U-Pb age of ca. 116 Ma on a carbonate from the Barra Velha Formation[37], given that the Macabu Formation can be directly correlated with the Barra Velha Formation based on $^{87}Sr/^{86}Sr$ ratios[86,87] (Supplementary Note 1). Core slabs and core plugs were prepared for sedimentology and organic–inorganic geochemistry analyses. Specifically, petrographic microscopic observations were carried out under plane-polarized, crossed-polarized and cathodoluminescence (CL) illumination on polished thin-sections. Several aliquots of bulk-rock powders were prepared for mineral (X-ray diffraction, XRD), isotopic and organic geochemistry analyses. To mitigate possible inorganic or organic contamination, the outer parts of core plugs were removed using a diamond blade saw. The inner parts, after gentle polishing, were then placed in a combusted jar and sonicated repeatedly with DI water for 15 seconds to remove the trace slurry on the fresh surfaces. Upon drying within a low-temperature oven (40 °C) they were ground in a puckmill. This was cleaned between samples to remove any potential cross-contaminating organic residues by first grinding an aliquot of combusted sand and then rinsing with DI water, MeOH and DCM (3X).

For each biomarker sample, approximately 2 g powdered sample was weighed and extracted (4X for 25 min at 100 °C) with dichloromethane (DCM): methanol (MeOH) (9:1;v:v) in a MARS 6 Microwave Digestion System at the Massachusetts Institute of Technology. The extracts were transferred into combusted 60 ml glass tubes using combusted pipettes, combined, and concentrated at room temperature under a gentle stream of N_2 on the TurboVap followed by transfer into combusted 4 ml vials with DCM rinsing and sonication. Elemental sulfur was removed by reaction with activated copper shot. The resultant extracts were dried to ~100 µl and fractionated using a silica gel column. Solvent mixtures of hexane: DCM (4:1; v:v) and DCM: MeOH (4:1;v:v) were used to elute the non-polar (free-NP) and polar fractions, sequentially.

Raney nickel desulfurization

For desulfurization reactions, "T-1" Raney-Nickel (RN) catalyst was prepared. Specifically, 40 g non-activated nickel aluminum alloy (1:1) was reacted with 600 ml of 10% sodium hydroxide for 1 h at the temperature of 95 °C under a gentle N_2 stream. Subsequently, the aqueous component was decanted and the residue washed with Milli-Q water (3X), and then activated by distilled absolute ethanol (3X). Natural ignition of dry Raney-Ni slurry verified the efficiency of prepared catalyst prior to use. Meanwhile, a procedure blank and an oil standard were subject to the procedure in each set of RN reactions. For desulfurization reactions, ~7 mg of the polar fraction of a TLE was dissolved in 20 ml distilled absolute ethanol together with 3 ml "T-1" RN slurry and the mixture heated to 80 °C under N_2 reflux for 2 h. The products were extracted into DCM with sonication (4X). After subsequent centrifugation and drying, aliquots of RN-treated new extracts were subjected to further silica gel column chromatography to obtain a second pair of NP (RN-NP) and polar fractions. RN reactivity and an absence of contamination were verified the recovery yields from an oil standard and the purity of blanks.

Lipid biomarker analysis

Both free-NP and RN-NP fractions were subjected to GC-MS analysis using a 7890B Agilent gas chromatograph coupled to a 5975 C Agilent MSD and a 7010 A Agilent triple quadrupole MS (GC-QQQ-MS) operated in full scan or multiple reaction monitoring (MRM) modes, respectively. All the GC's were equipped with a multi-mode injector at an initial injection temperature of 45 °C which was ramped at a rate of 720°/min to 340 °C. A DB-5MS column (60 m × 250 µm × 0.25 µm) was installed with each GC with an oven temperature held isothermally at 40° for 2 min, ramped to 320 °C at a rate of 4°/min, and then held at this temperature for 22 mins. The transfer lines and source temperatures in GC-MS and GC-QQQ-MS were set to 320 °C and 250 °C, respectively. The electron energy of GC-QQQ-MS was 70 eV to ensure a standard signal for the precursor-product transitions. All biomarker data are processed using MassHunter software. In GC-QQQ-MS, each compound was identified and integrated under MRM mode within a narrow retention time window (0.5 mins).

In situ $^{87}Sr/^{86}Sr$ analysis

The $^{87}Sr/^{86}Sr$ results were obtained by the LA-ICP-MS method at the University of Paraná, Brazil, with analytical resolution for the characterization of different phases, resolving micro structures varying between 2 µm and 150 µm. Results were obtained with excimer ArF laser ablation Analyte Excite CETAC Teledyne, generating beams with wavelength of 193 nm, which is sufficient energy to sample different carbonate microfacies. The ablation was carried out in raster mode, with sampling lines using laser beams with spot dimensions of 40 µm, in a path length of 700 µm, scanning speed of 10 µm/s, frequency of 7 Hz, and energy of 6.26 J/cm². The analyzes were carried out on ~1 mm fragments extracted from drill core plugs, which were previously analyzed by back-scattered electron (BSE) imaging using scanning electron microscopy analysis. The BSE images made it possible to accurately identify variations in composition such as silica replacement, clay minerals, fractures, and other relevant constituents for selecting the sampling area. Reproducibility was tested with three counter-tests per sample. Furthermore, samples from sample populations with end-member $^{87}Sr/^{86}Sr$ results were selected using the in-situ method, for further analysis and confirmation by ID-TIMS. The measurements were carried out in a multi collector ICP-MS Thermo Fischer Neptune Plus, monitoring the species ^{83}Kr (L4 amplifier 10^11), $^{167}Er^{+2}$ (L3 amplifier 10^13), ^{84}Sr (L2 amplifier 10^11), ^{85}Rb (L1 amplifier 10^11), ^{86}Sr (H1 amplifier 10^11), $^{173}Yb^{2+}$ (H2 amplifier 10^13), ^{87}Sr (H3 amplifier 10^11) and ^{88}Sr (H4 amplifier 10^11). As a reference standard, the coral JCp-1 was analyzed, which has an accepted $^{87}Sr/^{86}Sr$ ratio in the literature of 0.709160 ± 0.000020. The coral JCp-1 yielded a variable intensity of ^{88}Sr, the most abundant isotope, between 15 and 20 V measured with a 10^11 amplifier, equivalent to an estimated a Sr concentration from 7000 ppm to 2000 ppm, reflecting the heterogeneous distribution of strontium as it is a natural standard.

$\delta^{13}C$, $\delta^{18}O$ and clumped isotope (Δ_{47}) analysis of carbonate

Stable isotopic measurements of $\delta^{13}C$, $\delta^{18}O$, and carbonate clumped isotope (Δ_{47}) analyses were completed to contextualize the biomarker and $^{87}Sr/^{86}Sr$ results. Sample $\delta^{13}C$, $\delta^{18}O$, and Δ_{47} were measured from January 2020 to June 2021 at the MIT Carbonate Research Laboratory on a Nu Perspective dual-inlet isotope ratio mass spectrometer with a Nu Carb automated sample preparation unit held at 70 °C. Calcite samples weighing ~400–600 µg were reacted for 25 min in individual glass vials with 150 µl orthophosphoric acid ($\rho = 1.94$ g/cm^3). Evolved CO_2 gas was purified cryogenically and by passive passage through a Porapak trap (1/4" ID; 0.4 g 50/80 mesh Porapak Q) held at −30 °C. The initial voltage was 8–20 V on the m/z 44 beam with 2×10^8 Ω resistors and depleted by approximately 50% over the course of an analysis (60 cycles with 20-min total integration time). Sample and standard CO_2 gases depleted at equivalent rates from microvolumes over the analysis time. Mass spectrometry methods were nearly

identical to those reported in Anderson et al. (2021). ETH-1–4 and IAEA-C2 were used as anchors; IAEA-C1 and Merck were treated as unknowns. Unknown anchor ratio was 1:1 for each 50 run. The reference side of the dual-inlet was refilled with reference gas after every 10 analyses. In total, unknowns were measured 1–4 times over the study interval (76 total unknown analyses; 118 InterCarb standards). Raw mass spectrometer data were first processed by removing cycles (i.e., single integration cycles of mass spectrometer measurement) with raw Δ_{47} values more than 5 "long-term" standard deviations (0.50‰; the mean of the respective cycle-level SD for ETH-1–4 over a 3-month period was 0.10‰) away from the median Δ_{47} measurement for the analysis. Analyses were removed if more than 10 cycles (out of 60 total cycles) fell outside the 5 long-term SD threshold. Analyses with transducer pressure below 15 mbar, typically corresponding to sample collection issues, incomplete digestion, or low carbonate content, and analyses that ran misbalanced by >1% were also removed. No pressure baseline correction was applied. After removal of cycle-level outliers, data were processed using the 'D47crunch' Python package using IUPAC ^{17}O parameters[88], and projected to the I-CDES with values for ETH-1–4 and IAEA-C2 anchors from the InterCarb project[89,90]. Raw Δ_{47} measurements were converted to the I-CDES using a pooled-regression approach that accounts for the relative mapping of all samples in $\delta47$-Δ_{47} space[90]. Analytical uncertainty and error associated with the creation of the reference frame were fully propagated through the dataset. A full description of the data reduction procedure used in D47crunch is detailed in ref. 90. Each sample carousel (typically 50 analyses) was treated as a single analytical session. IAEA-C1 and Merck standards were treated as unknowns and used as an internal consistency check (IAEA-C1 mean $\Delta47 = 0.308$‰ vs. nominal $\Delta47 = 0.302$‰, 1 SD = 0.012‰; Merck mean $\Delta47 = 0.525$‰ vs. nominal $\Delta47 = 0.514$‰, 1 SD = 0.016‰). Long-term external repeatability (1 SD) of Δ_{47} for all analyses (anchors and unknowns) after the data processing described above, including error introduced by the reference frame, is 0.029‰.

Data availability

All data generated from this study are included in the article and Supplementary Inventory.

Received: 22 May 2024; Accepted: 13 January 2025;
Published online: 26 January 2025

References

1. Larson, R. L. & Ladd, J. W. Evidence for the opening of the South Atlantic in the Early Cretaceous. *Nature* **246**, 209–212 (1973).
2. Dias-Brito, D. Global stratigraphy, palaeobiogeography and palaeoecology of Albian–Maastrichtian pithonellid calcispheres: impact on Tethys configuration. *Cretac. Res.* **21**, 315–349 (2000).
3. Le Pichon, X. & Fox, P. J. Marginal offsets, fracture zones, and the early opening of the North Atlantic. *J. Geophys. Res.* **76**, 6294–6308 (1971).
4. Leandro, C. et al. Astronomical tuning of the Aptian stage and its implications for age recalibrations and paleoclimatic events. *Nat. Commun.* **13**, 1–12 (2022).
5. Santos, A. et al. Earlier onset of the Early Cretaceous Equatorial humidity belt. *Glob. Planet. Change* **208**, 103724 (2022).
6. Chaboureau, A.-C. et al. Paleogeographic evolution of the central segment of the South Atlantic during Early Cretaceous times: Paleotopographic and geodynamic implications. *Tectonophysics* **604**, 191–223 (2013).
7. Bastos, L. P. H. et al. Organic geochemical evidence for the transition of Aptian-Albian hypersaline environments into marine restricted seas: the South Atlantic oceanic northern gateway and its implications for the pre-salt deposits. *Mar. Pet. Geol.* **140**, 105632 (2022).
8. Arai, M. Aptian/Albian (Early Cretaceous) paleogeography of the South Atlantic: a paleontological perspective. *Braz. J. Geol.* **44**, 339–350 (2014).
9. Cui, X., Wignall, B., Freeman, K. H. & Summons, R. E. Early Cretaceous marine incursions into South Atlantic rift basins originated from the south. *Commun. Earth Environ.* **4**, 6 (2023).
10. Sanjines, A. E. S. et al. Planktonic foraminifera from the Aptian section of the Southeastern Brazilian Atlantic margin. *Cretac. Res.* **134**, 105141 (2022).
11. Bastos, L. P. H. et al. Expression of Early Cretaceous global anoxic events in Northeastern Brazilian basins. *Cretac. Res.* **110**, 104390 (2020).
12. Davison, I. Geology and tectonics of the South Atlantic Brazilian salt basins. *Geol. Soc., Lond., Spec. Publ.* **272**, 345–359 (2007).
13. Araripe, R. C., Oliveira, D. H., Tome, M. E., de Mello, R. M. & Barreto, A. M. Foraminifera and Ostracoda from the lower Cretaceous (Aptian–lower Albian) Romualdo formation, Araripe basin, northeast Brazil: Paleoenvironmental inferences. *Cretac. Res.* **122**, 104766 (2021).
14. Michels, F. H., de Souza, P. A. & Premaor, E. Aptian-Albian palynologic assemblages interbedded within salt deposits in the Espírito Santo Basin, eastern Brazil: biostratigraphical and paleoenvironmental analysis. *Mar. Pet. Geol.* **91**, 785–799 (2018).
15. Melo, R. M. et al. New marine data and age accuracy of the Romualdo Formation, Araripe Basin, Brazil. *Sci. Rep.* **10**, 1–15 (2020).
16. Dingle, R. Walvis Ridge barrier: its influence on palaeoenvironments and source rock generation deduced from ostracod distributions in the early South Atlantic Ocean. *Geol. Soc., Lond., Spec. Publ.* **153**, 293–302 (1999).
17. Heine, C., Zoethout, J. & Müller, R. D. Kinematics of the South Atlantic rift. *Solid Earth* **4**, 215–253 (2013).
18. Eagles, G. New angles on South Atlantic opening. *Geophys J. Int* **168**, 353–361 (2007).
19. Moulin, M., Aslanian, D. & Unternehr, P. A new starting point for the South and Equatorial Atlantic Ocean. *Earth-Sci. Rev.* **98**, 1–37 (2010).
20. Assine, M. L., Quaglio, F., Warren, L. V. & Simões, M. G. Comments on paper by M. Arai" Aptian/Albian (Early Cretaceous) paleogeography of the South Atlantic: a paleontological perspective". *Braz. J. Geol.* **46**, 03–07 (2016).
21. Peters K. E., Walters C. C. & Moldowan J. M. *The Biomarker Guide*. (Cambridge University Press, 2005).
22. Summons, R. E., Welander, P. V. & Gold, D. A. Lipid biomarkers: molecular tools for illuminating the history of microbial life. *Nat. Rev. Microbiol.* **20**, 174–185 (2022).
23. Roussel, A., Cui, X. & Summons, R. E. Biomarker stratigraphy in the Athel Trough of the South Oman Salt Basin at the Ediacaran-Cambrian Boundary. *Geobiology* **18**, 663–681 (2020).
24. Moldowan, J. M. C_{30}-steranes, novel markers for marine petroleums and sedimentary rocks. *Geochim Cosmochim. Acta* **48**, 2767–2768 (1984).
25. Moldowan, J. M. et al. Sedimentary 12-n-propylcholestanes, molecular fossils diagnostic of marine algae. *Science* **247**, 309–312 (1990).
26. McCaffrey, M. A. et al. Paleoenvironmental implications of novel C_{30} steranes in Precambrian to Cenozoic age petroleum and bitumen. *Geochim. Cosmochim. Acta* **58**, 529–532 (1994).
27. Ma J., et al Biomarkers reveal Eocene marine incursions into the Qaidam Basin, north Tibetan Plateau. *Organic Geochemistry* **166**,104380 (2022).
28. Xu, H., George, S. C. & Hou, D. The occurrence of isorenieratane and 24-n-propylcholestanes in Paleogene lacustrine source rocks from the Dongying Depression, Bohai Bay Basin: Implications for bacterial sulfate reduction, photic zone euxinia and seawater incursions. *Org. Geochem.* **127**, 59–80 (2019).
29. Hu, J. et al. Seawater incursion events in a Cretaceous paleo-lake revealed by specific marine biological markers. *Sci. Rep.* **5**, 1–6 (2015).
30. Kohnen, M. E., Damsté, J. S. S., Kock-van Dalen, A. & Jan, W. D. L. Di-or polysulphide-bound biomarkers in sulphur-rich geomacromolecules

as revealed by selective chemolysis. *Geochim. Cosmochim. Acta* **55**, 1375–1394 (1991).
31. Richnow, H., Jenisch, A. & Michaelis, W. Structural investigations of sulphur-rich macromolecular oil fractions and a kerogen by sequential chemical degradation. *Org. Geochem.* **19**, 351–370 (1992).
32. Schouten S., Eglinton T. I., Sinninghe Damsté J. S. & de Leeuw J. W. Influence of sulphur cross-linking on the molecular-size distribution of sulphur-rich macromolecules in bitumen). (ACS Publications, 1995).
33. Hebting, Y. et al. Biomarker evidence for a major preservation pathway of sedimentary organic carbon. *Science* **312**, 1627–1631 (2006).
34. Adam, P. et al. Structural investigation of nonpolar sulfur cross-linked macromolecules in petroleum. *Geochim Cosmochim. Acta* **57**, 3395–3419 (1993).
35. Kohnen, M. E., Sinninghe Damste, J. S. & De Leeuw, J. W. Biases from natural sulphurization in palaeoenvironmental reconstruction based on hydrocarbon biomarker distributions. *Nature* **349**, 775–778 (1991).
36. Schaeffer, P., Ocampo, R., Callot, H. & Albrecht, P. Extraction of bound porphyrins from sulphur-rich sediments and their use for reconstruction of palaeoenvironments. *Nature* **364**, 133–136 (1993).
37. Lawson, M. et al. New age and lake chemistry constraints on the Aptian pre-salt carbonates of the central South Atlantic. *Geol. Soc. Am. Bull.* **135**, 595–607 (2023).
38. Pietzsch, R. et al. Palaeohydrology of the Lower Cretaceous pre-salt lacustrine system, from rift to post-rift phase, Santos Basin, Brazil. *Palaeogeogr. Palaeoclimatol. Palaeoecol.* **507**, 60–80 (2018).
39. Jones, C. E. & Jenkyns, H. C. Seawater strontium isotopes, oceanic anoxic events, and seafloor hydrothermal activity in the Jurassic and Cretaceous. *Am. J. Sci.* **301**, 112–149 (2001).
40. Lima, B. E. M. & De Ros, L. F. Deposition, diagenetic and hydrothermal processes in the Aptian Pre-Salt lacustrine carbonate reservoirs of the northern Campos Basin, offshore Brazil. *Sediment. Geol.* **383**, 55–81 (2019).
41. Wright, V. P. & Barnett, A. J. The textural evolution and ghost matrices of the Cretaceous Barra Velha Formation carbonates from the Santos Basin, offshore Brazil. *Facies* **66**, 7 (2020).
42. Muniz, M. & Bosence, D. Lacustrine carbonate platforms: facies, cycles, and tectonosedimentary models for the presalt Lagoa Feia Group (Lower Cretaceous), Campos Basin, Brazil. *AAPG Bull.* **102**, 2569–2597 (2018).
43. Caetano-Filho, S., Dias-Brito, D., Rodrigues, R. & de Azevedo, R. L. M. Carbonate microfacies and chemostratigraphy of a late Aptian–early Albian marine distal section from the primitive South Atlantic (SE Brazilian continental margin): record of global ocean-climate changes? *Cretac. Res.* **74**, 23–44 (2017).
44. Giner, J. L., Zhao, H., Boyer, G. L., Satchwell, M. F. & Andersen, R. A. Sterol chemotaxonomy of marine pelagophyte algae. *Chem. Biodivers.* **6**, 1111–1130 (2009).
45. Volkman, J. Sterols in microorganisms. *Appl. Microbiol. Biotechnol.* **60**, 495–506 (2003).
46. Holba, A. et al. Application of tetracyclic polyprenoids as indicators of input from fresh-brackish water environments. *Org. Geochem.* **34**, 441–469 (2003).
47. Grabenstatter, J. et al. Identification of 24-n-propylidenecholesterol in a member of the Foraminifera. *Org. Geochem.* **63**, 145–151 (2013).
48. Pietzsch, R. et al. Environmental conditions of deposition of the Lower Cretaceous lacustrine carbonates of the Barra Velha Formation, Santos Basin (Brazil), based on stable carbon and oxygen isotopes: a continental record of pCO2 during the onset of the Oceanic Anoxic Event 1a (OAE 1a) interval? *Chem. Geol.* **535**, 119457 (2020).
49. Farias, F., Szatmari, P., Bahniuk, A. & França, A. B. Evaporitic carbonates in the pre salt of Santos Basin: genesis and tectonic implications–A reply. *Mar. Pet. Geol.* **133**, 105201 (2021).
50. Louback, V. S., de Castro Valente, S., de Almeida, C. N., Ross, J. & Borghi, L. Aptian flood basalts in Bacalhau oil and gas field: petrogenesis and geodynamics of post-rift tholeiites in the pre-salt sequence of Santos Basin, Brazil. *Contrib. Mineral. Petrol.* **178**, 1–25 (2023).
51. Bralower, T., Fullagar, P., Paull, C., Dwyer, G. & Leckie, R. Mid-Cretaceous strontium-isotope stratigraphy of deep-sea sections. *Geol. Soc. Am. Bull.* **109**, 1421–1442 (1997).
52. Farias, F., Szatmari, P., Bahniuk, A. & Franca, A. B. Evaporitic carbonates in the pre-salt of Santos Basin–Genesis and tectonic implications. *Mar. Pet. Geol.* **105**, 251–272 (2019).
53. Dummann, W., Hofmann, P., Herrle, J. O., Frank, M. & Wagner, T. The early opening of the Equatorial Atlantic gateway and the evolution of Cretaceous peak warming. *Geology* **51**, 476–480 (2023).
54. Coolen, M. J. et al. Evolution of the plankton paleome in the Black Sea from the Deglacial to Anthropocene. *Proc. Natl Acad. Sci.* **110**, 8609–8614 (2013).
55. Sinninghe Damsté, J. S. et al. The identification of mono-, di-and trimethyl 2-methyl-2-(4,8,12-trimethyltridecyl) chromans and their occurrence in the geosphere. *Geochim. Cosmochim. Acta* **51**, 2393–2400 (1987).
56. Tulipani, S. et al. Molecular proxies as indicators of freshwater incursion-driven salinity stratification. *Chem. Geol.* **409**, 61–68 (2015).
57. Sinninghe Damsté, J. K. et al. Variations in abundances and distributions of isoprenoid chromans and long-chain alkylbenzenes in sediments of the Mulhouse Basin: a molecular sedimentary record of palaeosalinity. *Org. Geochem.* **20**, 1201–1215 (1993).
58. Harvey, H. R. & Mcmanus, G. B. Marine ciliates as a widespread source of tetrahymanol and hopan-3β-ol in sediments. *Geochim. Cosmochim. Acta* **55**, 3387–3390 (1991).
59. Sinninghe Damsté, J. S. et al. Evidence for gammacerane as an indicator of water column stratification. *Geochim. Cosmochim. Acta* **59**, 1895–1900 (1995).
60. Didyk, B., Simoneit, B., Brassell, S. T. & Eglinton, G. Organic geochemical indicators of palaeoenvironmental conditions of sedimentation. *Nature* **272**, 216–222 (1978).
61. Grice, K., Schouten, S., Nissenbaum, A., Charrach, J. & Damsté, J. S. S. Isotopically heavy carbon in the C21 to C25 regular isoprenoids in halite-rich deposits from the Sdom Formation, Dead Sea Basin, Israel. *Org. Geochem.* **28**, 349–359 (1998).
62. Tulipani, S., Grice, K., Greenwood, P. & Schwark, L. A pyrolysis and stable isotopic approach to investigate the origin of methyltrimethyltridecylchromans (MTTCs). *Org. Geochem.* **61**, 1–5 (2013).
63. Sinninghe Damsté, J. S., Kok, M. D., Köster, J. & Schouten, S. Sulfurized carbohydrates: an important sedimentary sink for organic carbon? *Earth Planet. Sci. Lett.* **164**, 7–13 (1998).
64. Sinninghe Damsté, J., Van Duin, A. C., Hollander, D., Kohnen, M. E. & De Leeuw, J. W. Early diagenesis of bacteriohopanepolyol derivatives: Formation of fossil homohopanoids. *Geochim. Cosmochim. Acta* **59**, 5141–5157 (1995).
65. Gomez-Saez, G. V. et al. Sulfurization of dissolved organic matter in the anoxic water column of the Black Sea. *Sci. Adv.* **7**, eabf6199 (2021).
66. Raven, M. R., Sessions, A. L., Adkins, J. F. & Thunell, R. C. Rapid organic matter sulfurization in sinking particles from the Cariaco Basin water column. *Geochim Cosmochim. Acta* **190**, 175–190 (2016).
67. Ma, J., Cui, X., Liu, X.-l, Wakeham, S. G. & Summons, R. E. Rapid sulfurization obscures carotenoid distributions in modern euxinic environments. *Geochim. Cosmochim. Acta*. **380**, 180–193 (2024).
68. Ma J., French K. L., Cui X., Bryant D. A., & Summons R. E. Carotenoid biomarkers in Namibian shelf sediments: Anoxygenic photosynthesis during sulfide eruptions in the Benguela Upwelling System. *Proc. Natl. Acad. Sci. USA* **118**, e2106040118 (2021).
69. Sinninghe Damsté, J. & Koopmans, M. The fate of carotenoids in sediments: an overview. *Pure Appl. Chem.* **69**, 2067–2074 (1997).
70. Schwark, L. & Empt, P. Sterane biomarkers as indicators of Palaeozoic algal evolution and extinction events. *Palaeogeogr., Palaeoclimatol., Palaeoecol.* **240**, 225–236 (2006).

71. Kirst, G. Salinity tolerance of eukaryotic marine algae. *Annu. Rev. plant Biol.* **41**, 21–53 (1990).
72. Imhoff J. F. Taxonomy and physiology of phototrophic purple bacteria and green sulfur bacteria. In: *Anoxygenic photosynthetic bacteria*. (Springer, 1995).
73. Repeta, D., Simpson, D., Jorgensen, B. & Jannasch, H. Evidence for anoxygenic photosynthesis from the distribution of bacterio-chlorophylls in the Black Sea. *Nature* **342**, 69–72 (1989).
74. Cui, X. et al. Niche expansion for phototrophic sulfur bacteria at the Proterozoic–Phanerozoic transition. *Proc. Natl Acad. Sci.* **117**, 17599–17606 (2020).
75. French, K., Rocher, D., Zumberge, J. & Summons, R. Assessing the distribution of sedimentary C 40 carotenoids through time. *Geobiology* **13**, 139–151 (2015).
76. Ma J., Cui X. Aromatic carotenoids: Biological sources and geological implications. *Geosystems and Geoenvironment*, 100045 (2022).
77. Summons, R. E. & Powell, T. G. Chlorobiaceae in Palaeozoic seas revealed by biological markers, isotopes and geology. *Nature* **319**, 763–765 (1986).
78. Sinninghe Damsté, J. S., Schouten, S. & Van Duin, A. C. Isorenieratene derivatives in sediments: possible controls on their distribution. *Geochim. Cosmochim. Acta* **65**, 1557–1571 (2001).
79. Overmann, J., Cypionka, H. & Pfennig, N. An extremely low-light adapted phototrophic sulfur bacterium from the Black Sea. *Limnol. Oceanogr.* **37**, 150–155 (1992).
80. Vila, X. & Abella, C. Effects of light quality on the physiology and the ecology of planktonic green sulfur bacteria in lakes. *Photosynth. Res.* **41**, 53–65 (1994).
81. Block, K. R., O'Brien, J. M., Edwards, W. J. & Marnocha, C. L. Vertical structure of the bacterial diversity in meromictic Fayetteville Green Lake. *MicrobiologyOpen* **10**, e1228 (2021).
82. Peduzzi, S., Tonolla, M. & Hahn, D. Isolation and characterization of aggregate-forming sulfate-reducing and purple sulfur bacteria from the chemocline of meromictic Lake Cadagno, Switzerland. *FEMS Microbiol. Ecol.* **45**, 29–37 (2003).
83. Wilbanks, E. G. et al. Microscale sulfur cycling in the phototrophic pink berry consortia of the S ippewissett S alt M arsh. *Environ. Microbiol.* **16**, 3398–3415 (2014).
84. Graham, J. E. & Bryant, D. A. The biosynthetic pathway for synechoxanthin, an aromatic carotenoid synthesized by the euryhaline, unicellular cyanobacterium Synechococcus sp. strain PCC 7002. *J. Bacteriol.* **190**, 7966–7974 (2008).
85. Graham, J. E., Lecomte, J. T. & Bryant, D. A. Synechoxanthin, an aromatic C40 xanthophyll that is a major carotenoid in the cyanobacterium Synechococcus sp. PCC 7002. *J. Nat. Prod.* **71**, 1647–1650 (2008).
86. Winter, W. R., Jahnert, R. J. & França, A. B. Bacia de campos. *Bol. de. Geociências da Petrobras* **15**, 511–529 (2007).
87. Moreira, J. L. P., Madeira, C. V., Gil, J. A. & Machado, M. A. P. bacia de Santos. *Bol. de. Geocienc. da Petrobras* **15**, 531–549 (2007).
88. Kim, S.-T., O'Neil, J. R., Hillaire-Marcel, C. & Mucci, A. Oxygen isotope fractionation between synthetic aragonite and water: Influence of temperature and Mg2+ concentration. *Geochim. Cosmochim. Acta* **71**, 4704–4715 (2007).
89. Bernasconi, S. M. et al. InterCarb: a community effort to improve interlaboratory standardization of the carbonate clumped isotope thermometer using carbonate standards. *Geochem. Geophys. Geosyst.* **22**, e2020GC009588 (2021).
90. Daëron, M. Full propagation of analytical uncertainties in Δ47 measurements. *Geochem. Geophys. Geosyst.* **22**, e2020GC009592 (2021).
91. Seifert, W. K. & Moldowan, J. M. The effect of biodegradation on steranes and terpanes in crude oils. *Geochim. Cosmochim. Acta* **43**, 111–126 (1979).
92. Sandison, C. M., Alexander, R. & Kagi, R. I. The analysis of polar fractions from sediment extracts and crude oils using reaction-gas chromatography–mass spectrometry. *Org. Geochem.* **34**, 1373–1389 (2003).

Acknowledgements

Financial support at the Massachusetts Institute of Technology (MIT) was provided by an MIT Energy Initiative grant funded by Shell with additional support from the Simons Foundation Collaboration on the Origins of Life that provided instrumentation needed for this work. Funding support at Shanghai Jiao Tong University (SJTU) is provided by the National Natural Science Foundation of China (42203030, 42273075), the Shanghai Pujiang Programme and the SJTU startup grant (WH220544005). We are grateful to Shell for allowing sample access to the Fragata well.

Author contributions

J.M., R.E.S. L.F.C., and A.M.B.R. designed the research; J.M., R.E.S., X.C., and H.L.A. performed the biomarker analysis; L.F.C. and K.S conducted Sr isotopic analysis; K.D.B., A.M.B.R., E.W.A., J.E.A., and A.G.C. performed C, O, clumped isotopic and petrographic analyses. J.M. and R.E.S. wrote the draft, and all authors have contributions on revising the manuscript.

Competing interests

The authors declare no competing interests.

Additional information

Supplementary information The online version contains supplementary material available at https://doi.org/10.1038/s43247-025-02029-2.

Correspondence and requests for materials should be addressed to Jian Ma or Roger E. Summons.

Peer review information *Communications Earth and Environment* thanks Lucas Bastos and Jose Manuel Castro for their contribution to the peer review of this work. Primary Handling Editor: Carolina Ortiz Guerrero. A peer review file is available.